Available online at www.sciencedirect.com
ScienceDirect
Phytochemistry 68 (2007) 2243–2257
PHYTOCHEMISTRY
www.elsevier.com/locate/phytochem

Flux quantification in central carbon metabolism of *Catharanthus roseus* hairy roots by ^{13}C labeling and comprehensive bondomer balancing

Ganesh Sriram [a,1], D. Bruce Fulton [b], Jacqueline V. Shanks [a,*]

[a] *Department of Chemical and Biological Engineering, 3031 Sweeney Hall, Iowa State University, Ames, IA 50011, USA*
[b] *Department of Biophysics, Biochemistry, and Molecular Biology, Iowa State University, Ames, IA 50011, USA*

Received 28 November 2006; received in revised form 29 March 2007
Available online 25 May 2007

Abstract

Methods for accurate and efficient quantification of metabolic fluxes are desirable in plant metabolic engineering and systems biology. Toward this objective, we introduce the application of "bondomers", a computationally efficient and intuitively appealing alternative to the commonly used isotopomer concept, to flux evaluation in plants, by using *Catharanthus roseus* hairy roots as a model system. We cultured the hairy roots on (5% w/w U–^{13}C, 95% w/w naturally abundant) sucrose, and acquired two-dimensional [^{13}C, ^{1}H] and [^{1}H, ^{1}H] NMR spectra of hydrolyzed aqueous extract from the hairy roots. Analysis of these spectra yielded a data set of 116 bondomers of β-glucans and proteinogenic amino acids from the hairy roots. Fluxes were evaluated from the bondomer data by using comprehensive bondomer balancing. We identified most fluxes in a three-compartmental model of central carbon metabolism with good precision. We observed parallel pentose phosphate pathways in the cytosol and the plastid with significantly different fluxes. The anaplerotic fluxes between phosphoenolpyruvate and oxaloacetate in the cytosol and between malate and pyruvate in the mitochondrion were relatively high (60.1 ± 2.5 mol per 100 mol sucrose uptake, or 22.5 ± 0.5 mol per 100 mol mitochondrial pyruvate dehydrogenase flux). The development of a comprehensive flux analysis tool for this plant hairy root system is expected to be valuable in assessing the metabolic impact of genetic or environmental changes, and this methodology can be extended to other plant systems.

Keywords: Plant metabolic flux; *Catharanthus roseus*; Hairy roots; Bondomer; Compartmented metabolism; Anaplerotic flux; Plant metabolic engineering

1. Introduction

Metabolic flux quantification facilitates the understanding of carbon trafficking in plants. Fluxes are important determinants of cell physiology (Stephanopoulos, 1999; Sauer, 2004), and collectively represent the phenotype of an organism (Ratcliffe and Shachar-Hill, 2005). Comparative flux measurements between phenotypes can provide valuable insights toward the manipulation of phenotypes (Ratcliffe and Shachar-Hill, 2006), the elucidation of metabolic control (Stephanopoulos, 2002; Stephanopoulos and Stafford, 2002; Sweetlove and Fernie, 2005), and the construction of predictive models of plant metabolism (Ratcliffe and Shachar-Hill, 2001; Sweetlove et al., 2003). Therefore, the systemwide measurement of fluxes can complement transcriptomic, proteomic and metabolomic profiling technologies as a powerful investigative tool in plant systems biology (Sweetlove et al., 2003; Lange, 2006). Furthermore, since substantial changes in flux sometimes correspond only to minor changes in metabolite levels (Fell, 2005), systemwide flux quantification is a very useful counterpart to the profiling of metabolite concentrations (through metabolomics) in the characterization of phenotype (Ratcliffe and Shachar-Hill, 2006).

* Corresponding author. Tel.: +1 515 294 4828; fax: +1 515 294 2689.
E-mail address: jshanks@iastate.edu (J.V. Shanks).
[1] Present address: Department of Human Genetics and Department of Chemical and Biomolecular Engineering, University of California, Los Angeles 695, Charles E. Young Dr. South #5335, Los Angeles, CA 90095, USA.

0031-9422/$ - see front matter © 2007 Elsevier Ltd. All rights reserved.
doi:10.1016/j.phytochem.2007.04.009

Flux quantification in plants is challenging compared to that in microbial and mammalian cells. This is largely because flux quantification involves performing labeling experiments and interpreting the ensuing labeling data by mathematical techniques, and such techniques grow to be quite non-trivial in case of plant metabolism due to its inherent complexity, subcellular compartmentation, and intercompartmental transport (Ratcliffe and Shachar-Hill, 2001; Shanks, 2005; Rhee et al., 2006). Consequently, flux quantification in plants through labeling experiments has received limited attention (Kruger et al., 2003; Sweetlove et al., 2003; Fernie et al., 2005), although a few elegant examples of the use of labeling experiments for pathway elucidation or discovery have been reported (e.g. Wheeler et al., 1998; Kruger et al., 2003; Schwender et al., 2004a). Encouragingly, flux quantification in plants is gradually gaining pace, as exemplified by recent articles demonstrating the use of carbon atom enrichment and isotopomer data to evaluate fluxes (Rontein et al., 2002; Schwender et al., 2003, 2004b, 2007; Sriram et al., 2004; Spielbauer et al., 2006). In a recent publication (Sriram et al., 2004), we reported the systemwide evaluation of compartmented fluxes in soybean (*Glycine max*) embryos by using isotopomer data and a generic computational framework employing comprehensive isotopomer balancing.

In this article, we introduce the application of bondomers and bondomer balancing to flux quantification in plants. The bondomer (“bond isomer”) concept (Sriram and Shanks, 2001, 2004; van Winden et al., 2002) is a computationally efficient alternative to the popular isotopomer (“isotope isomer”) concept in interpreting data from labeling experiments employing a single fractionally U–^{13}C labeled carbon source (Sriram and Shanks, 2004; Ratcliffe and Shachar-Hill, 2006). Bondomer data also afford easier interpretation than isotopomer data. Bondomers are isomers of a metabolite that differ in the connectivity (intact versus biosynthetic) of their carbon–carbon bonds (Fig. 1). A bond between two consecutive carbon atoms in a metabolite is defined “intact” or “unbroken” if those atoms originated from the same molecule of the carbon source and the bond between them was unbroken during metabolism. Conversely, a bond between two consecutive carbon atoms is defined “biosynthetic” if those atoms originated from distinct molecules of the carbon source and the bond between them was biosynthetically assembled during metabolism (Sriram and Shanks, 2004). A linear metabolite with n carbon atoms has 2^n isotopomers and 2^{n-1} bondomers. For this and other reasons, a given metabolic network has fewer bondomers than isotopomers. Bondomers and NMR-detectable isotopomers are interconvertible and provide identical metabolic information in an experiment using a single U–^{13}C substrate. Therefore, bondomer balancing is computationally efficient and saves significant flux evaluation time. Further, bondomers afford a more intuitive interpretation of labeling data than isotopomers. This is because isotopomer data contain *both* metabolic flux information and labeling experiment information

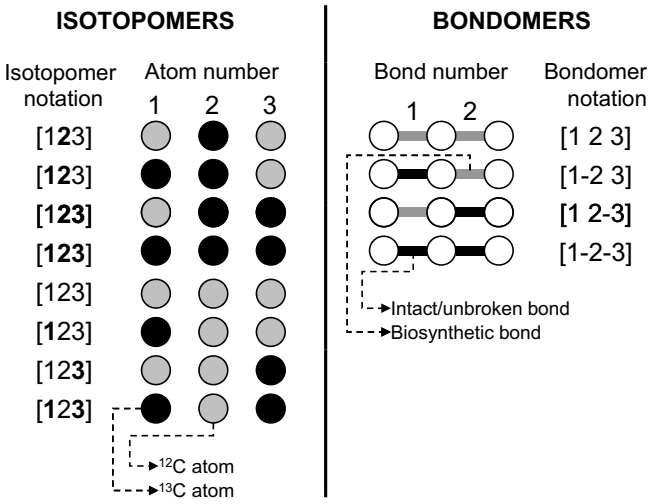

Fig. 1. Isotopomers (isotope isomers) and bondomers (bond isomers) of a three-carbon metabolite. All eight isotopomers (left) and all four bondomers (right) of this metabolite are shown. The isotopomers differ in the labeling state of their individual carbon atoms [^{13}C (black) versus ^{12}C (gray)]. They are notated using boldface for ^{13}C and regular font for ^{12}C, as illustrated. Bondomers differ in the connectivity of their carbon–carbon bonds [intact or unbroken (black) versus biosynthetic (gray)]. Two consecutive carbon atoms in a metabolite linked by an intact bond originated from the same carbon substrate molecule and the bond between them was unbroken during metabolism. Whereas, two consecutive carbon atoms linked by a biosynthetic bond originated from different carbon substrate molecules and were biosynthetically assembled during metabolism. Bondomers are notated using a dash (1–2) for an intact bond and no dash (1 2) for a biosynthetic bond, as illustrated. A linear metabolite with n carbon atoms has 2^n isotopomers and 2^{n-1} bondomers. For this and other reasons, a given metabolic network has fewer bondomers than isotopomers. Bondomers provide identical flux information as NMR-detectable isotopomers in an experiment using a single fractionally U–^{13}C labeled carbon source. Bondomers save significant flux evaluation time and are more easily interpretable than isotopomers.

(extent of labeling and natural abundance of ^{13}C); however bondomer data contain *purely* metabolic flux information (Sriram and Shanks, 2004).

We employed biosynthetically directed fractional ^{13}C labeling (Szyperski, 1995) and comprehensive bondomer balancing to evaluate fluxes through central carbon metabolism in *Catharanthus roseus* hairy roots. This is a model plant system of pharmaceutical significance and produces high-value terpenoid indole alkaloids (TIAs), some of which possess therapeutic properties (Bhadra and Shanks, 1997). It is an attractive metabolic engineering target since the natural production of indole alkaloids by the hairy roots is very low. Recently, engineering of *C. roseus* hairy roots for TIA overproduction has resulted in several genetic variants (Hughes et al., 2004b; Hong et al., 2006a) that are promising candidates for the application of flux analysis and consequent metabolic reengineering. This work accomplished the development of a metabolic flux analysis tool to investigate the metabolism of a tissue type (hairy roots) wherein metabolic fluxes have not been previously analyzed in detail. We expect this tool to be useful in characterizing genetic variants of the hairy roots that

have been engineered to overexpress anthranilate synthase, tryptophan decarboxylase, and other enzymes intended to enhance TIA overproduction (Hughes et al., 2004c; Hong et al., 2006a), which can be expected to have an effect on primary metabolism. For example, in tobacco, the overexpression of tryptophan decarboxylase had a substantial effect on upstream pathways (Guillet et al., 2000).

Our results showed parallel pentose phosphate pathways in the cytosol and the plastid with significantly different fluxes, and high anaplerotic fluxes. To the extent of our knowledge, this is the first application of bondomer theory in flux analysis of a compartmented metabolic or plant system, and the first ^{13}C labeling-based flux analysis of a plant hairy root system.

2. Results

We cultured *C. roseus* hairy roots on fractionally U–^{13}C labeled sucrose by transferring five hairy root tips to Gamborg B5/2 media containing 5% (w/w) U–^{13}C sucrose as the sole carbon source. These root tips exhibited normal growth and lateral branching, and were visually indistinguishable from controls grown on unlabeled sucrose. The growth rate and extracellular fluxes of the 5% U–^{13}C sucrose-grown hairy roots were not significantly different from those of the unlabeled sucrose-grown controls (data not shown; $p > 0.30$, $n = 4$).

2.1. 2-D [^{13}C, ^{1}H] HSQC spectra, fine structures, and isotopomer abundances

We measured isotopomer abundances of biomass components of *C. roseus* hairy roots and evaluated bondomer abundances from the isotopomer abundances. To measure isotopomer abundances, we obtained an aqueous extract of *C. roseus* hairy roots grown on 5% U–^{13}C sucrose, acid hydrolyzed the extract, and acquired two-dimensional (2-D) [^{13}C, ^{1}H] heteronuclear single quantum correlation (HSQC) spectra of the hydrolysate (e.g. Fig. 2a). Herein, we identified carbon atoms of 16 amino acids, levulinic acid (LVA), and hydroxyacetone (HyA). Unequivocal identification of these carbon atoms was possible due to their unique $^{13}C/^{1}H$ chemical shifts, distinctive coupling patterns, and *J*-coupling constants (J_{CC}) (Harris, 1983; Sriram et al., 2004). Because protein was detected in the aqueous

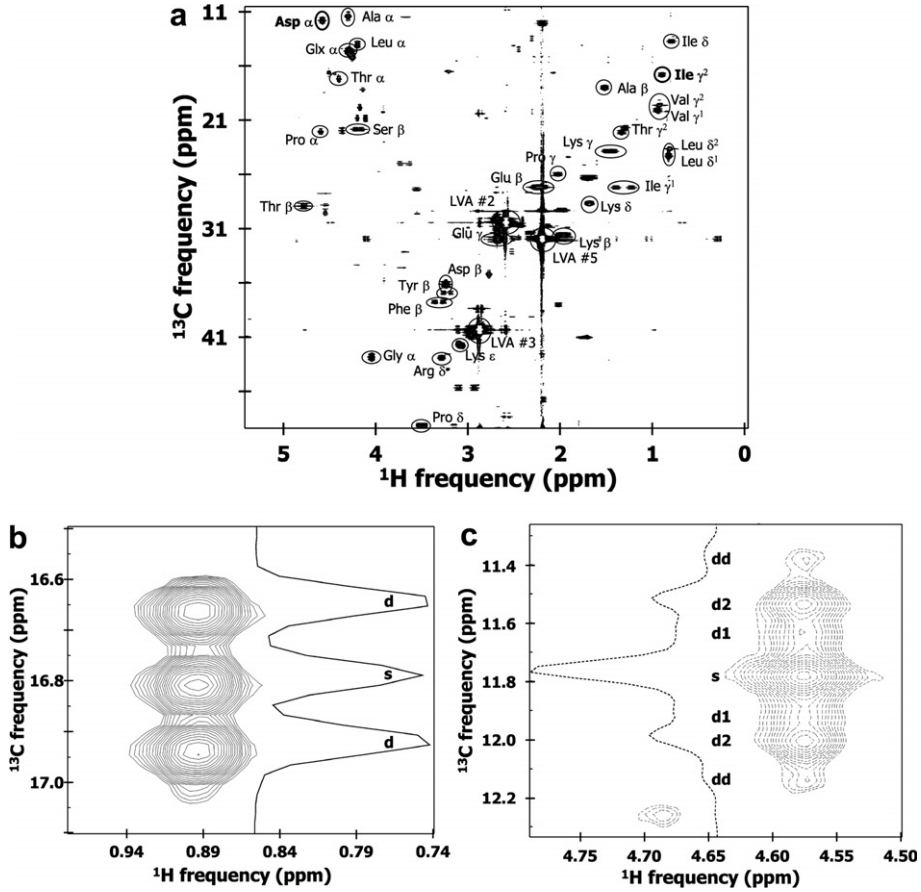

Fig. 2. (a) 2-D [^{13}C, ^{1}H] HSQC spectrum of hydrolyzed aqueous extract of *C. roseus* hairy roots grown on (5% w/w U–^{13}C) sucrose. Cross-peaks represent carbon atoms of hydrolysate constituents (proteinogenic amino acids, LVA, HyA). The names of some amino acid nuclei are omitted for clarity. Expanded views of (b) Ile γ^2, and (c) Asp α cross-peaks. One-dimensional slices are shown alongside. The multiplet peaks are *s*: singlet; *d*, *d*1, *d*2: doublet; *dd*: double doublet.

extract (data not shown), the amino acids identified in its hydrolysate resulted from degradation of the protein under the hydrolysis conditions (145 °C, vacuum, 6 N HCl). Hence, they are proteinogenic amino acids that were mostly synthesized in the hairy roots during the labeling experiment. The LVA and HyA peaks appeared on the spectrum because aqueous extracts of mid-exponential phase *C. roseus* hairy roots contain mostly β-glucans (~95% w/w; Sriram et al., 2006), which are polymers of glucose. Under the hydrolysis conditions employed, the hexose skeleton of glucose is converted to LVA and HyA (Sriram G, Iyer VV, Shanks JV, unpublished data).

The cross-peaks in the [^{13}C, ^{1}H] spectrum displayed peak splitting along the ^{13}C dimension, due to ^{13}C–^{13}C scalar coupling. This is evident in expanded views of the cross-peaks, e.g. Ile γ^2 (Fig. 2b) and Asp α (Fig. 2c). These satellite peaks observed in the fine structure of a cross-peak are termed multiplets, and each multiplet represents a particular isotopomer of the detected compound (Sriram et al., 2004). For instance, in the Ile γ^2 cross-peak (Fig. 2b), the central singlet peak (s) represents a population of Ile isotopomers in which the γ^2 atom has a ^{13}C nucleus and the β atom adjacent to it has a ^{12}C nucleus. Whereas, the two doublet peaks (d) distributed on either side of the singlet together represent a population of Ile isotopomers in which both the γ^2 and β atoms have ^{13}C nuclei. Using the isotopomer notation explained in Fig. 1, the isotopomer population corresponding to the singlet may be represented as [$\beta\gamma^2$], and the one corresponding to the doublet as [$\boldsymbol{\beta\gamma}^2$]. Likewise, the fine structure of the Asp α cross-peak shows a singlet (*s*), a doublet (*d*1), a doublet (*d*2) and a double doublet (*dd*) (Fig. 2c). As per the isotopomer notation in Fig. 1, the isotopomer populations corresponding to these multiplets are: singlet, [C$\alpha\beta$x]; doublet *d*1, [C$\boldsymbol{\alpha\beta}$x]; doublet *d*2, [**C**$\alpha\boldsymbol{\beta}$x]; double doublet, [**C**$\boldsymbol{\alpha\beta}$x]. Here 'C' and 'β' stand for the carboxyl and β atoms adjacent to the Asp α atom, and 'x' stands for an undeterminable labeling state, i.e. the labeling state of the atom represented by 'x' (Asp γ) cannot be detected from the Asp α fine structure.

The abundances of the isotopomer populations represented by the multiplets are directly proportional to the integrals of the respective multiplet peaks. We quantified peak integrals by various methods depending on the complexity of the fine structure (see Section 5), to obtain 116 relative isotopomer abundances of proteinogenic amino acids, LVA, and HyA (Supplementary material 1).

2.2. 5% U–^{13}C sucrose is uniformly incorporated into hairy roots

We quantified the extent of ^{13}C label incorporation into the 5% U–^{13}C sucrose-grown hairy roots by acquiring a 2-D [^{1}H, ^{1}H] total correlation (TOCSY) spectrum of acid hydrolyzed aqueous extract of the hairy roots (not shown). Cross-peaks on this spectrum corresponded to protons of the constituents of the hydrolysate (proteinogenic amino acids, LVA, and HyA identified in the [^{13}C, ^{1}H] HSQC spectra above). These cross-peaks displayed peak splitting along both ^{1}H dimensions. From the resultant multiplets, we quantified positional ^{13}C enrichments of the carbon atoms attached to the detected protons as explained in Schmidt et al. (1999; who used correlation spectroscopy, COSY, instead of TOCSY). The average ^{13}C enrichment across the carbon atoms of the proteinogenic amino acids and β-glucans was 5.52 ± 0.33%. This agrees well with the expected value (5.60%) calculated from the ^{13}C enrichment of the carbon source (5% w/w), natural ^{13}C abundance (1.1%), and dilution (9%) by initially present unlabeled hairy root biomass. Therefore, the uptake of the ^{13}C label into proteinogenic amino acids and β-glucans was uniform and in the same ^{13}C:^{12}C proportion as in the growth medium.

2.3. Bondomer abundances

We converted the isotopomer abundances measured from the [^{13}C, ^{1}H] HSQC spectra to bondomer abundances of metabolic precursors by using retrobiosynthetic reconstruction, statistical relationships from Szyperski (1995), and the extent of ^{13}C labeling (5.52 ± 0.33%) determined above. To illustrate, the β and γ^2 atoms of Ile are respectively synthesized from atoms 2 and 3 of pyruvate (Pyr). Therefore, the abundances of the Pyr[2**3**] and Pyr[**23**] isotopomers are respectively equal to those of the isotopomers Ile[$\beta\boldsymbol{\gamma}^2$] (=0.33 ± 0.00) and Ile[$\boldsymbol{\beta\gamma}^2$] (=0.67 ± 0.00). Further, the Pyr[2**3**] and Pyr[**23**] isotopomer abundances are related to the Pyr[2 3] and Pyr[2–3] bondomer abundances through statistical relationships derived in Szyperski (1995). Using these relationships and the measured extent of ^{13}C labeling, we calculated the abundance of the Pyr[2 3] bondomer to be 0.19 ± 0.00 and that of the Pyr[2–3] bondomer to be 0.81 ± 0.00. In this manner, we evaluated 116 relative bondomer abundances (listed in Supplementary material 1).

The bondomer abundances provide many interesting insights into metabolic flux patterns, as illustrated below. Five out of the six OAA bondomers (as derived from Asp) were not significantly different ($p > 0.05$, Fig. 3a) from the OAA^{p} bondomers (derived from Met, Ile, Lys, and Thr), with the single exception being the [1 2 3] bondomers, which were slightly, but significantly different with $p = 0.04$ (possibly due to their low standard deviations). Since plants synthesize Asp from cytosolic, plastidic and mitochondrial OAA but synthesize Met, Ile, Lys, and Thr exclusively from plastidic oxaloacetate (OAA^{p}) (Singh, 1999), this observation indicates that the OAA^{p} pool and the OAA pools in other compartments have very similar metabolic history. The OAA^{p} bondomers derived from Thr α were not considered in the above comparison because the Thr α signal on the 2-D HSQC spectrum had significant noise, and this made the quantification of isotopomers/bondomers from this cross-peak rather difficult (Supplementary material 1). However, the OAA^{p}[3 4] and OAA^{p}[3–4] bondomers derived from Thr γ^2 did not exhibit

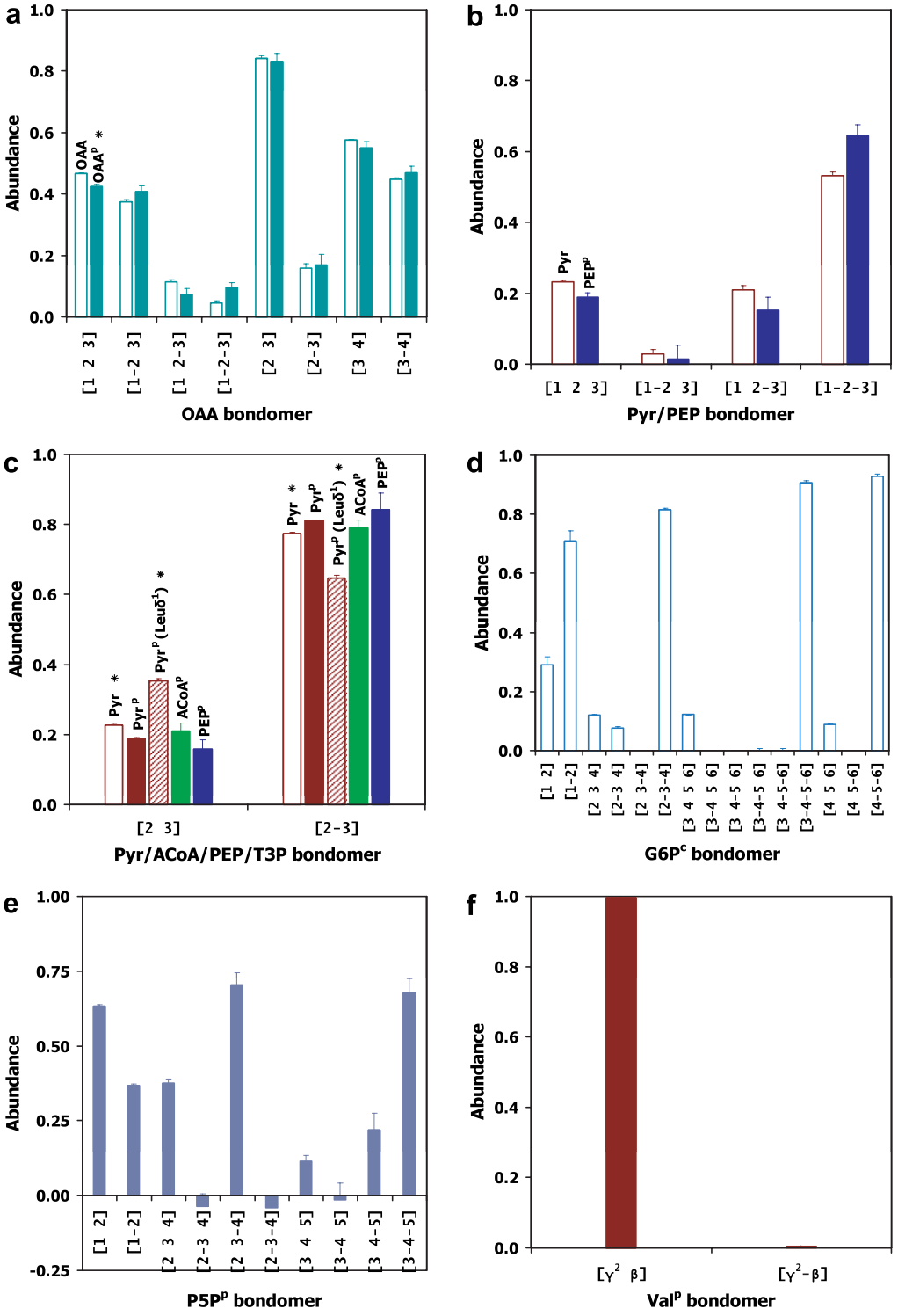

Fig. 3. Selected bondomer abundances of intracellular precursor metabolites in *C. roseus* hairy roots grown on (5% w/w U–^{13}C) sucrose. Bondomer abundances were retrobiosynthetically evaluated from measured isotopomer abundances of sink metabolites (proteinogenic amino acids, LVA, HyA) from [^{13}C, ^{1}H] spectra, and are reported as fractions of the corresponding metabolite pool. Error bars represent standard errors estimated as described in Materials and Methods. Bondomers are grouped by metabolic precursor, as follows: (a) OAA (evaluated from Asp α and Asp β) and OAA^{p} (evaluated from Met α, Ile δ, Ile γ^1, Lys γ, and Thr γ^2); (b) Pyr (from Ala α) and PEP^{p} (from Phe α); (c) Pyr (from Ala β, Ile γ^2, Leu δ^1) and neighboring metabolites ACoA^{p} (from Leu α)/PEP (from Phe β and Tyr β); (d) G6P^{c} (from LVA); (e) P5P^{c} (from His); (f) Val^{p}. '*' denotes bondomer abundances that are significantly different ($p < 0.05$) from the rest of the group. A superscript 'p' indicates that the metabolite is located in the plastid, the absence of a superscript indicates that compartmentation could not be unambiguously determined. Metabolite abbreviations: OAA (oxaloacetate), Pyr (pyruvate), PEP (phosphoenolpyruvate), ACoA (acetyl CoA), G6P (glucose-6-phosphate), P5P (pentose-5-phosphate). In the online version of this article, bondomers are color-coded as in Supplementary Material 1.

this problem, and were in agreement with other OAA^p[3 4] and OAA^p[3 4] bondomers derived from Ile, Lys, and Met (Supplementary material 1).

Similarly, the bondomer abundances of Pyr evaluated from Ala α were not significantly different from those of phosphoenolpyruvate (PEP) evaluated from Phe α and Tyr α ($p > 0.05$, Fig. 3b), although there was a small but significant difference between the corresponding [2–3] bondomers, possibly due to the very small standard deviations of the [2–3] bondomers. Since plants synthesize Ala from cytosolic, plastidic and mitochondrial Pyr but synthesize Phe and Tyr only from plastidic phosphoenolpyruvate (PEP^p), (Singh, 1999) this observation indicates that the successive three-carbon metabolites PEP and Pyr in the cytosol and the plastid have very similar metabolic history. The abundances of the bondomers PEP^p[2–3], Pyr[2–3], plastidic pyruvate (Pyr^p)[2–3], and plastidic acetyl CoA ($ACoA^p$) [2–3] evaluated from various amino acids were statistically similar (Fig. 3c), indicating that these consecutive glycolytic metabolites have the same metabolic history, whether located in the cytosol or the plastid. However, Leu δ^1 was a notable exception: the Pyr^p[2–3] bondomer abundance evaluated from Leu δ^1 (0.65 ± 0.00) was significantly different ($p < 0.01$) from that evaluated from other amino acids Ile or Val (0.81 ± 0.00) synthesized from Pyr^p (Fig. 3c).

The bondomers of cytosolic glucose-6-phosphate ($G6P^c$), evaluated from β-glucan-generated LVA and HyA, were mostly intact (Fig. 3d). This suggests that the non-oxidative pentose phosphate pathway (n-oxPPP) in the cytosol was either non-existent or had very low activity. The n-oxPPP includes carbon skeleton-rearranging reactions that can produce biosynthetic G6P bondomers. In contrast, biosynthetic bondomers of plastidic pentose-5-phosphate ($P5P^p$) were abundant (Fig. 3e). Particularly, the abundances of the $P5P^p$ bondomers that have an intact bond between carbon atoms 2 and 3 ($P5P^p$[2–3 4] and $P5P^p$[2–3–4]) were not statistically different from zero. This is a hallmark of the transketolase reaction in the n-oxPPP (Szyperski, 1995) and therefore suggests that the n-oxPPP was relatively active in the plastid. Therefore, the bondomer abundances suggest parallel pentose phosphate pathways (PPP) in the cytosol and the plastid, with different fluxes in their n-oxPPP branches. The cytosolic n-oxPPP flux is either zero (the observed biosynthetic bonds could be due to equilibration by G6P from the plastid) or very low compared to that in the plastid.

The β and γ^2 atoms of Val are synthesized from distinct Pyr^p molecules (Szyperski, 1998); therefore, the bond between them should always be biosynthetic irrespective of the metabolic fluxes affecting the bondomer abundances of Pyr^p. Not surprisingly, the abundances of the Val[β γ^2] and Val[β–γ^2] bondomers were 1.00 ± 0.00 and 0.00 ± 0.00, respectively (Fig. 3f). This provides a consistency check for our evaluation of bondomer abundances from the NMR data.

2.4. Direct calculation of anaplerotic flux from bondomer abundances

Bondomer abundances enable the straightforward calculation of fluxes at certain branchpoints in metabolism, in an approach that is analogous to the MetaFoR approach introduced previously (Fiaux et al., 1999; Sauer et al., 1999). For instance, the relative contributions of the two pathways that synthesize OAA can be determined directly from the abundance of the OAA[2–3] bondomer. The two pathways for OAA synthesis [tricarboxylic (TCA) cycle and anaplerotic pathway] are depicted in Fig. 4. In the TCA cycle (flux v_1), OAA is synthesized from citrate, which is itself synthesized from OAA and ACoA. This pathway always synthesizes OAA with a biosynthetic bond between carbon atoms 2 and 3 (OAA[2 3]). In the anaplerotic pathway (flux v_2), OAA is synthesized from PEP and CO_2. Here, PEP[2–3] results in OAA with an intact [2–3] bond, whereas PEP[2 3] results in OAA with a biosynthetic [2 3] bond.

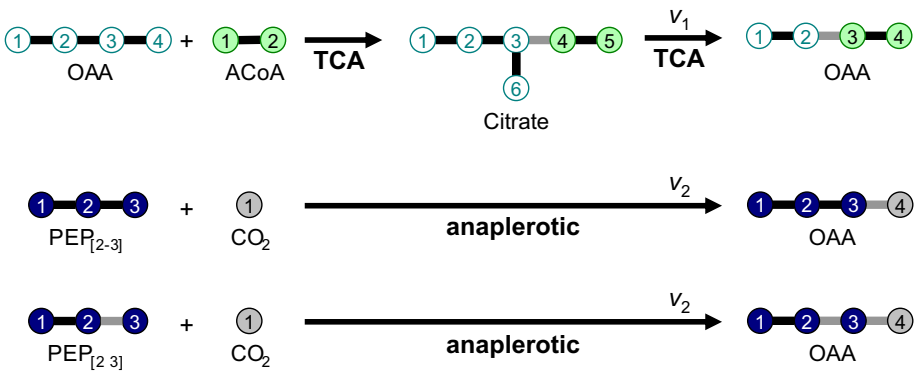

Fig. 4. Two pathways for OAA synthesis. In the first (TCA cycle; flux v_1), OAA is synthesized from citrate, which is itself synthesized from OAA and ACoA. This pathway always synthesizes OAA with a biosynthetic [2–3] bond. In the second (anaplerotic pathway; flux v_2), OAA is synthesized from PEP and CO_2. In this pathway, PEP[2–3]/PEP[2–3], respectively, produce OAA with an intact/biosynthetic [2–3] bond. Metabolite abbreviations: OAA (oxaloacetate), PEP (phosphoenolpyruvate), ACoA (acetyl CoA). In the online version of this article, reactant metabolites (OAA, ACoA) and the OAA/citrate atoms originating from them are color-coded as in Supplementary Material 1.

Therefore, a steady state bondomer balance (Sriram and Shanks, 2004) for the OAA[2–3] bondomer can be written as

$$\sum(\text{influxes}) = \sum(\text{effluxes}), \tag{1}$$

or

$$v_2 \cdot \text{PEP}_{[2-3]} = (v_1 + v_2) \cdot \text{OAA}_{[2-3]}. \tag{2}$$

On rearrangement, this gives

$$\frac{v_2}{v_1 + v_2} = \frac{\text{OAA}_{[2-3]}}{\text{PEP}_{[2-3]}}. \tag{3}$$

The left-hand side represents the fractional contribution of the anaplerotic pathway to OAA synthesis, or the relative flux of the anaplerotic pathway at the OAA branchpoint. Substituting the bondomer abundances of OAA[2–3] (derived from Asp α and Asp β) and PEP[2–3] (derived from Phe α) (Supplementary material 1) into Eq. (3), we determined the relative flux of the anaplerotic pathway to be 21 ± 1%.

2.5. Extracellular and biomass synthesis fluxes

During hairy root growth on 5% U–^{13}C sucrose, measurements of extracellular fluxes (those between the hairy roots and the growth medium) were as follows. The biomass growth rate was 4.70 ± 0.7 mg d^{-1} flask^{-1}, and the biomass dry weight at harvest time was 0.0775 g flask^{-1}. The sucrose uptake rate was 21.1 ± 0.2 mg d^{-1} flask^{-1}, or 0.80 ± 0.01 mmol d^{-1} g^{-1} biomass. During mid-exponential phase, sucrose was the only metabolite detected in the medium. Glucose, fructose, Pyr, malate (Mal), and succinate were below HPLC-detectable levels, and therefore the fluxes of their production by the hairy roots were negligible. This is consistent with previous work from our laboratory (Bhadra and Shanks, 1997), except that 3 mM formate was detected in that work. Biomass synthesis fluxes were determined in a previous work (Sriram et al., 2006) from the measured biomass composition of the *C. roseus* hairy roots in mid-exponential phase of growth.

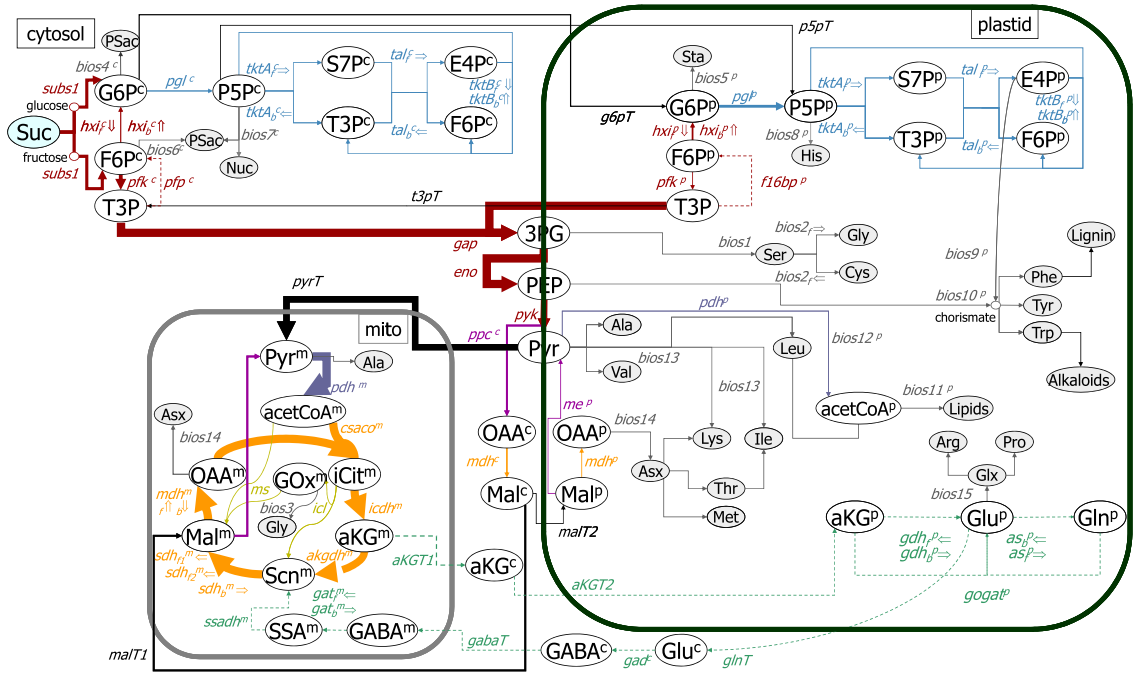

Fig. 5. Flux map of primary and intermediate metabolism in *C. roseus* hairy roots grown on (5% w/w U–^{13}C) sucrose. Arrow widths are directly proportional to fluxes. Dashed lines indicate fluxes that could not be identified satisfactorily. A table containing values and standard deviations of fluxes is provided in Supplementary Material 2. Intracellular metabolites are shown in white ovals, and gray ovals show sink metabolites (e.g. proteinogenic amino acids, polysaccharides) that are components of biomass. Metabolic pathways are color-coded as follows: dark red (glycolysis and sucrose metabolism), pale blue (pentose phosphate pathway), orange (TCA cycle), blue-gray (pyruvate dehydrogenase link), mauve (anaplerotic fluxes), dark yellow (glyoxylate shunt), green (glutamate metabolism, GABA shunt, and associated intercompartmental transport fluxes), gray (fluxes towards biomass synthesis), and black (all intercompartmental transport fluxes except those involved in Gln metabolism and GABA shunt). F6P and T3P appear at two different locations each in the cytosol and the plastid to reduce intersections of lines. Each flux is assigned a short name based on the name of the gene encoding one of the metabolic reactions represented by it. Intracellular metabolites and fluxes with a superscript are located in specific subcellular compartments: c (cytosol), p (plastid), m (mitochondrion). If a flux is has no superscript, its compartmentation could not be unambiguously determined (such as *gap*, *eno* and *pyk*, and some fluxes toward biosynthesis). Intracellular metabolite abbreviations: Suc (sucrose), G6P (glucose-6-phosphate), F6P (fructose-6-phosphate), T3P (triose-3-phosphate), P5P (pentose-5-phosphate), S7P (sedoheptulose-7-phosphate), E4P (erythrose-4-phosphate), 3PG (3-phosphoglycerate), PEP (phospho *enol* pyruvate), Pyr (pyruvate), acetCoA (acetyl CoA), iCit (isocitrate), aKG (α-ketoglutarate), Scn (succinate), Mal (malate), OAA (oxaloacetate), GABA (γ-aminobutyric acid), SSA (succinic semi-aldehyde), GOx (glyoxylate). Sink metabolite abbreviations: PSac (glucose polysaccharides/β-glucans), Nuc (carbon skeleton of nucleotides), Sta (starch). Asp and Asn are denoted together as Asx. Glu and Gln are denoted together as Glx.

2.6. Metabolic fluxes

From the measured bondomer abundances, extracellular fluxes and biomass synthesis fluxes, we evaluated 84 metabolic fluxes in a three-compartmental model of central carbon metabolism. Our metabolic model consisted of glycolysis, PPP, and TCA cycle, as well as anaplerotic fluxes, glyoxylate, and γ-aminobutyric acid (GABA) shunts. Effluxes to the shikimate pathway and onward to lignin and TIA biosynthesis were also included (Fig. 5). Photosynthesis, photorespiration, and the Calvin cycle were excluded from the model since *C. roseus* hairy roots are heterotrophic. Employing bondomer balancing or isotopomer balancing to evaluate fluxes resulted in an identical flux solution, as expected. However, bondomer balancing was 4.3-fold faster than isotopomer balancing.

The evaluated metabolic fluxes are depicted in Fig. 5 (where arrow widths are directly proportional to flux). Fluxes of key metabolic pathways and reactions are shown in Fig. 6, and a complete listing is available in Supplementary material 2. Fig. 7 depicts the correlation between experimental bondomer abundances and those simulated from the evaluated fluxes. Clearly, the evaluated fluxes account for the experimental bondomer abundances well, with Leu δ^1 bondomers being the only major exception.

Most fluxes were well-identified with nominal standard deviations, except for fluxes in the GABA shunt and the flux through fructose-1,6-bisphosphatase in the plastid ($f16bp^p$). Fluxes of parallel pathways in separate compartments (e.g. cytosolic and plastidic PPP) were quantified with good precision. The flux through the oxidative pentose phosphate pathway (oxPPP) in the cytosol was 0.34 ± 0.11 mmol d^{-1} g^{-1} biomass or 42.6 ± 13.2 mol per 100 mol sucrose uptake, while that through the plastidic oxPPP was 0.74 ± 0.22 mmol d^{-1} g^{-1} biomass or 92.5 ± 27.6 mol per 100 mol sucrose uptake. The fluxes through the cytosolic n-oxPPP (0.07 ± 0.03 mmol d^{-1} g^{-1} biomass) and the plastidic n-oxPPP (0.30 ± 0.09 mmol d^{-1} g^{-1} biomass) were significantly different ($p < 0.01$). Conversely, the fluxes through the lower glycolytic pathway [triose-3-phosphate (T3P) to Pyr] in the cytosol and the plastid were not distinguishable, since the three-carbon intermediates of this pathway (PEP and Pyr) from the cytosol or the plastid had the same metabolic history (Fig. 3b, c). Therefore, only their combined flux is reported. The anaplerotic flux from PEP to OAA in the cytosol (0.48 ± 0.02 mmol d^{-1} g^{-1} biomass) as well as that from Mal to Pyr in the mitochondrion (0.49 ± 0.03 mmol d^{-1} g^{-1} biomass) were substantial. The flux through the glyoxylate shunt was negligible (0.02 ± 0.02 mmol d^{-1} g^{-1} biomass). What the model identified as plastidic malic enzyme flux (me^p) is a malic enzyme flux that was distinct from the mitochondrial malic enzyme flux. This non-mitochondrial malic enzyme flux could be, strictly, either cytosolic or plastidic as per the isotopic data; however, it is distinct from the mitochondrial malic enzyme flux. Similarly, the phosphoenolpyruvate carboxykinase flux detected by the model could be either cytosolic or plastidic, but because this enzyme is cytosolic (Chollet et al.,

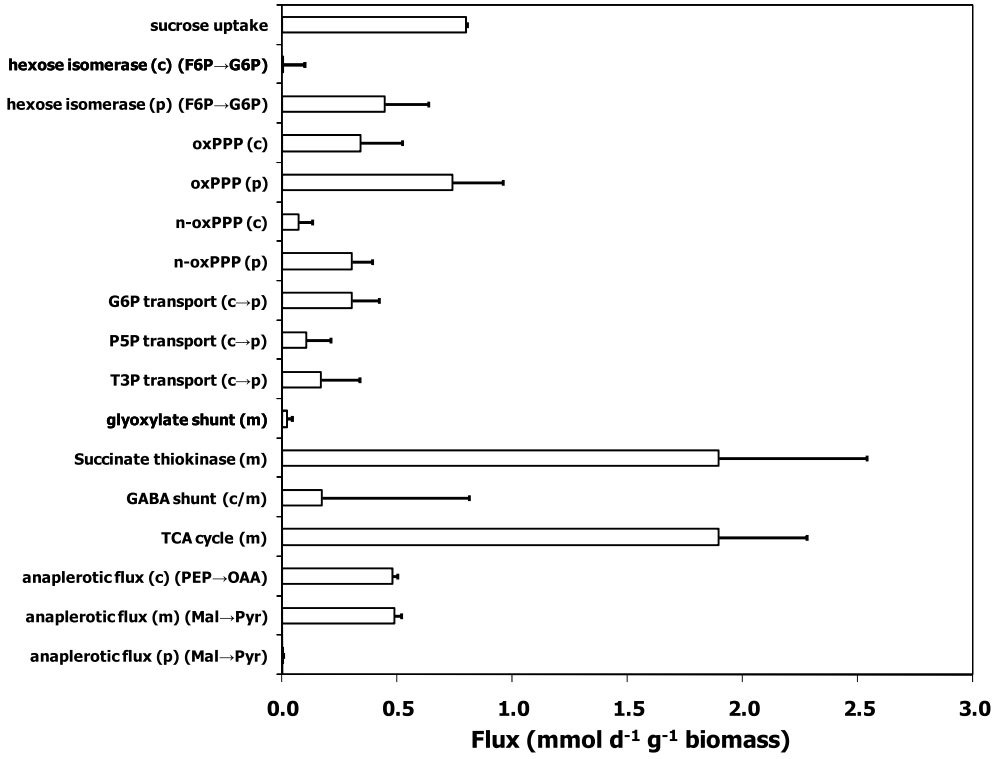

Fig. 6. Selected metabolic fluxes in for *C. roseus* hairy roots grown on (5% w/w U–^{13}C) sucrose. Absolute fluxes are expressed in mmol d^{-1} g biomass^{-1}. Error bars represent standard deviations of the fluxes evaluated as described in Section 5.

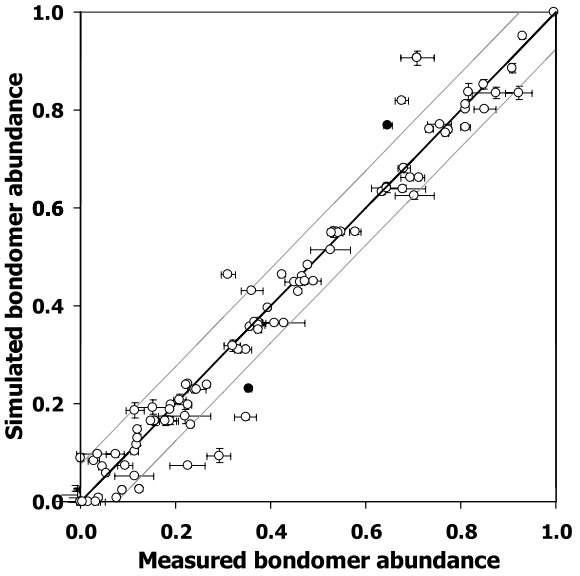

Fig. 7. Comparison of experimental and simulated bondomer abundances, portraying how closely the evaluated fluxes account for the experimental bondomer abundances. The *x*-axis represents experimental bondomer abundances, obtained by converting isotopomer abundances measured from [^{13}C, ^{1}H] spectra (error bars represent standard deviations derived from measured signal:noise ratios of the spectra); the *y*-axis represents bondomer abundances that were simulated by the computer program NMR2Flux, corresponding to the evaluated fluxes of Figs. 5 and 6 (error bars represent standard deviations of the simulated intensities from 200 simulations). Bondomer abundances are shown as fractions of the corresponding metabolite pool. The thick diagonal line is the 45° diagonal, on which the error between measurement and simulation is zero. The thin lines enclose 90% of all data points (all points with error $\leqslant$0.0540). The bondomer abundances of Leu δ^1 are shown as closed circles.

1996), we have designated the corresponding flux as cytosolic.

3. Discussion

In this article, we introduce the use of bondomers, a computationally efficient and intuitively interpretable alternative to isotopomers, to quantify metabolic fluxes in a plant system. Because the isotopomer and bondomer data obtained in this work were interconvertible, we could evaluate metabolic fluxes by employing either bondomer balancing or isotopomer balancing. As expected, the results of both methods were statistically identical (i.e. identical within the standard deviations of the fluxes as estimated by either method). Hence, the fluxes obtained from either method were not statistically different from each other ($p \gg 0.05$). Flux evaluation using bondomer balancing was substantially (4.3-fold) faster than that using isotopomer balancing. This is because bondomer/isotopomer balancing is the slowest step in flux evaluation. Since the number of bondomers in a given metabolic network is fewer than the number of isotopomers [usually by an order of magnitude (Sriram and Shanks, 2004)], bondomer balancing is a significantly faster process than isotopomer balancing. Because flux evaluation in plants is computationally demanding due to the intrinsic complexity of plant metabolism, the reduction in computation time facilitated by the use of bondomer balancing is a valuable benefit (Sriram and Shanks, 2004; Ratcliffe and Shachar-Hill, 2006). This advantage should be more evident during the application of instationary flux analysis to plants. Instationary flux analysis (Wiechert and Nöh, 2005; Nöh and Wiechert, 2006), an emerging technique that could have wide application in plants, is computationally highly demanding and could benefit from the use of efficient techniques such as bondomer balancing.

Besides being a computationally efficient alternative to isotopomers, bondomers are also more intuitively interpretable. This is because isotopomer data contain both metabolic flux information and labeling experiment information (extent of labeling and natural abundance of ^{13}C); however bondomer data contain purely metabolic flux information. Statistical relationships derived in Szyperski (1995) that convert isotopomer data to bondomer data essentially decouple labeling experiment information from metabolic flux information. The intuitive interpretability of bondomers enables the direct, accurate calculations of fluxes at certain branchpoints in metabolism without having to implement comprehensive bondomer balancing. For instance, we used bondomer abundances derived from Asp α, Asp β, and Phe α to calculate the relative flux of the anaplerotic pathway at the OAA branchpoint, and obtained the result $21 \pm 1\%$. This is not significantly different from the value evaluated later by comprehensive bondomer balancing, $23 \pm 1\%$ (Supplementary material 2).

However, comprehensive bondomer balancing is indispensable in the evaluation of fluxes through more complex pathways that involve bidirectional reactions (such as glycolysis and PPP). For example, when the "local bondomer" approach is applied to the OAA[3 4]/OAA[3–4] bondomers instead of the OAA[2 3]/OAA[2–3] bondomers, it gives an (apparently) incorrect result for value of the anaplerotic flux. This is because the [1–2] and [3–4] bonds of OAA can likely be equilibrated by the bidirectional reactions OAA ↔ Mal ↔ fumarate/succinate (where OAA and Mal are asymmetric molecules while fumarate and succinate are symmetrical molecules). This is especially so when the above bidirectional reactions are fairly rapid compared to the TCA cycle and anaplerotic reactions (Klapa et al., 1999). This equilibration significantly affects the abundances of the OAA[3 4]/OAA[3–4] bondomers (which are at the end of the OAA molecule) due to asymmetry, but does not affect those of the OAA[2 3]/OAA[2–3] bondomers (which are at the center of the OAA molecule) due to symmetry. Therefore, anaplerotic flux calculations using the "local bondomer" approach are quite straightforward when the OAA[2 3]/OAA[2–3] bondomers (that are not affected by reversibilities of bidirectional reactions) are used, but complicated when the OAA[3 4]/OAA[3–4]

bondomers (that are affected by reversibilities) are used. This is why we did not illustrate the local bondomer approach with the OAA[3 4]/OAA[3–4] bondomers.

Four practical requirements for the accurate quantification of fluxes from a ^{13}C labeling experiment are normal growth on the ^{13}C–^{12}C carbon source mixture, uniform incorporation of this mixture into biomass, the attainment of isotopic steady state, and the existence of a metabolic steady state during the course of the experiment. *C. roseus* hairy roots grown on 5% U–^{13}C sucrose satisfied the first two of these criteria well (see Section 2). To verify isotopic steady state, we examined the extent of incorporation of ^{13}C into proteinogenic amino acids and β-glucan during the labeling experiment. The extent of ^{13}C incorporation was 98.5 ± 5.8% of the steady state value (see Section 2), which verifies that isotopic steady state was attained over the course of the labeling experiment. Furthermore, we calculated the residence time of sucrose in the hairy roots from the measured sucrose uptake rate (0.80 mmol d^{-1} g^{-1} biomass), and the intracellular concentration of sucrose in the hairy roots [~0.15 mmol g^{-1} biomass; Schlatmann et al. (1995)]. The evaluated residence time was 0.19 d. Since isotopic steady state is usually attained in five residence times (~1 d) and the 16.5 d labeling period employed in this work is substantially higher than this, the residence time calculation provides an additional confirmation of isotopic steady state attainment. Therefore, all the labeling data obtained in this work can be assumed to be at isotopic steady state. Metabolic steady state is partially verified by constant slopes of extracellular fluxes during the mid-exponential phase (Bhadra and Shanks, 1997) and constancy of cell protein composition during different growth phases (Sriram et al., 2006). However, the strictest verification of metabolic steady state would involve measurement of isotopomer/bondomer abundances and consequent flux estimation at different times during the 16.5 d period of the experiment. This was not performed in this work due to the prohibitive cost of U–^{13}C sucrose, but may be feasible in the future after the development of more sensitive isotopomer measurement techniques. Therefore, the fluxes estimated in this work are an average of the fluxes in the hairy roots during the period of the labeling experiment.

Flux identifiability, the prospect of being able to find a unique flux solution from the labeling data, is an important computational requirement of ^{13}C labeling-based metabolic flux analyses. In this work, we identified most central metabolic fluxes in three compartments from bondomer abundances of metabolites in a single analyte (acid hydrolysate of aqueous extract of hairy roots). The few fluxes that were not well-identified were those in the GABA shunt and gluconeogenic fluxes from T3P to F6P through $f16bp^p$ (plastid) and pfp^c (cytosol). The GABA shunt fluxes were not identifiable because a labeling experiment employing U–^{13}C sucrose as the sole carbon source will produce indistinguishable isotopomer patterns for TCA cycle intermediates irrespective of the flux through GABA (Sriram and Shanks, unpublished calculations). The $f16bp^p$ and pfp^c fluxes could not be identified since we did not measure isotopomer abundances from starch hydrolysate, which is necessary to quantify flux through $f16bp^p$ (Sriram et al., 2004; Iyer et al., 2007). Nevertheless, non-green heterotrophic plant tissues such as *C. roseus* hairy roots are not expected to contain $f16bp^p$, whose primary function is the conversion of photosynthate to starch (Entwistle and ap Rees, 1990). However, the estimated values of the cytosolic and plastidic oxPPP fluxes were not affected by the inclusion or omission of the gluconeogenic $f16bp^p$ and pfp^c fluxes – we calculated oxPPP fluxes using metabolic models that both included and did not include the reverse flux from 2 T3P to F6P (in both the cytosol and the plastid), and both models gave the same (cytosolic and plastidic) oxPPP fluxes within the same standard deviations.

Our bondomer data suggested that fluxes through the cytosolic and plastidic n-oxPPPs were different – the cytosolic n-oxPPP had a small flux, whereas the plastidic n-oxPPP had a relatively higher flux. This was confirmed by flux evaluation with comprehensive bondomer balancing. Conversely, the fluxes through the lower glycolytic pathway in the cytosol and the plastid were not distinguishable (Fig. 5, Table 1). This suggests that *C. roseus* hairy roots may contain a single lower glycolytic pathway common to the cytosol and the plastid. This finding is consistent with previous findings (Table 1) in soybean embryos (Sriram et al., 2004) and *Brassica napus* embryos (Schwender et al., 2003), and as discussed Sriram et al. (2004), it may be a feature of metabolism in many higher plants.

Interestingly, we found many differences (Table 1) in metabolic flux patterns between *C. roseus* hairy roots, and plant systems previously analyzed in detail: soybean embryos (Sriram et al., 2004) and *Brassica napus* embryos (Schwender et al., 2003). For example, the oxPPP flux in *C. roseus* hairy roots, although lower than that in soybean, was higher than that in *B. napus* (Table 1). In addition, the amount of NADPH supplied by the (plastidic) oxPPP as a percentage of NADPH demand by biosynthetic pathways was very high in *C. roseus* hairy roots as compared to the other two systems (Table 1). This points other sinks for plastidic NADPH such as combating oxidative stress. Amongst mitochondrial fluxes, the flux through the TCA cycle in *C. roseus* hairy roots was considerably larger than that in the other two plant systems, indicating respiration as a principal metabolic activity in *C. roseus* hairy roots during mid-exponential phase. However, the glyoxylate shunt flux was negligible in *C. roseus* as well as the other two plant systems, which is expected since the glyoxylate shunt is usually turned on only in germinating (not growing) embryos and in leaves during senescence.

We observed rather high anaplerotic fluxes from PEP to OAA in the cytosol and Mal to Pyr in the mitochondrion (48.1 mmol d^{-1} g^{-1} biomass; alternatively, 60.1 ± 2.5 mol per 100 mol sucrose uptake, 30.0 ± 1.2 mol per mol of uptake of glucose equivalents, or 22.5 ± 0.5 mol per 100 mol mitochondrial pyruvate dehydrogenase flux). These fluxes constitute the elementary flux mode

Table 1
Comparison of key metabolic flux ratios between mid-exponential *Catharanthus roseus* hairy roots (this work), canola (*Brassica napus*) embryos (Schwender et al., 2003, 2004b, 2007), and soybean (*Glycine max*) embryos (Sriram et al., 2004)

	Catharanthus roseus hairy roots (this work)	Canola (*Brassica napus*) embryos	Soybean (*Glycine max*) embryos
oxPPP flux (cytosol + plastid) relative to uptake of glucose equivalents (%)	67 ± 13	37 ± 13	104 ± 23
NADPH supplied by (plastidic) oxPPP as a proportion of NADPH demand by biosynthetic pathways (%)	356 ± 107	22 to 45	98 ± 45
Non-oxidative PPP flux (cytosol) relative to uptake of glucose equivalents (%)	4 ± 2	12 ± 4	3 ± 1
Non-oxidative PPP flux (plastid) relative to uptake of glucose equivalents (%)	19 ± 6		28 ± 8
Separate 'lower' glycolytic pathways (T3P → → Pyr) identified in cytosol and plastid?	No	No	No
TCA cycle (mitochondrion) flux relative to uptake of glucose equivalents (%)	129 ± 4	10 ± 1	27 ± 7
Cytosolic phosphoenolpyruvate carboxykinase (ppc^c) flux, relative to TCA cycle (%)	23 ± 1	64 ± 5	42 ± 6
Mitochondrial malic enzyme (me^m) flux, relative to TCA cycle (%)	23 ± 1	41 ± 5	18 ± 8
Mitochondrial malic enzyme (me^m) flux, relative to uptake of glucose equivalents (%)	30 ± 1	1 ± 0	4 ± 2
Glyoxylate shunt (ms^m) flux, relative to TCA cycle (%)	1 ± 1	0	0 ± 0

$PEP^c \rightarrow OAA^c \rightarrow Mal^c \rightarrow Mal^m \rightarrow Pyr^m$ (anaplerotic mode), which is an alternative to the usual elementary flux mode through pyruvate dehydrogenase (*pdh*), $PEP^c \rightarrow Pyr^c \rightarrow Pyr^m$ (*pdh* mode). On a sucrose/glucose uptake basis, the flux through the anaplerotic mode in *C. roseus* hairy roots is much higher than that in soybean embryos (Sriram et al., 2004) or *Brassica napus* embryos (Schwender et al., 2007).

It is well-known that the usual role of anaplerotic fluxes is to support export of organic acids from the TCA cycle for synthesis of the aspartate family of amino acids. However, the amount of anaplerotic flux measured by us (48.1 mmol d^{-1} g^{-1} biomass) is very substantial compared to that expected (0.2 mmol d^{-1} g^{-1} biomass) if anaplerotic fluxes played only this TCA cycle-replenishment role. A likely explanation for such a high flux is that the anaplerotic mode enables transport of reductant (NADH or NADPH) from the cytosol to the mitochondrion, and that actively respiring mid-exponential phase *C. roseus* hairy roots may require a high supply of reductant in the mitochondrion. For every 1 mol of flux through the anaplerotic mode, cytosolic malate dehydrogenase (that catalyzes $OAA^c \rightarrow Mal^c$) consumes 1 mol cytosolic NAD(P)H, whereas mitochondrial malic enzyme (that catalyzes $Mal^m \rightarrow Pyr^m$) produces 1 mol mitochondrial NAD(P)H. Therefore, this mode indirectly facilitates the intercompartmental transport of NAD(P)H (Zoglowek et al., 1988; King and Opie, 1998), which by itself cannot cross membranes (van Gulik et al., 2000). On the contrary, the *pdh* mode does not effect NAD(P)H transport. The NAD(P)H transported into the mitochondrion by the anaplerotic mode may lower the cytosolic NAD(P)H/$NAD(P)^+$ ratio and/or supplement the mitochondrial NAD(P)H provided by the TCA cycle for respiration. The respiration flux of the mid-exponential phase hairy roots was substantial (933 ± 8.5 mol per 100 mol sucrose uptake, or ~78% of the sucrose intake on a weight basis), and this high flux may necessitate additional mitochondrial NAD(P)H than what could be provided by the TCA cycle. From the evaluated fluxes (Supplementary material 2), we calculated the NAD(P)H provided by the anaplerotic mode (0.48 ± 0.02 mmol d^{-1} g biomass^{-1}) to be ~8% that provided by the TCA cycle (6.05 ± 0.18 mmol d^{-1} g biomass^{-1}).

The bondomer abundances of the Pyr^p[2 3] and Pyr^p[2–3] bondomers derived from Leu δ^1 were significantly different from those derived from other amino acids (Ile or Val) synthesized from Pyr^p (Fig. 3c). Moreover, the Leu δ^1 bondomer abundances were the largest contributors to the χ^2 error (26.7% of the χ^2 error) between the experimental and simulated bondomer abundances (Fig. 7). We have also observed this anomaly reproducibly in soybean embryos (Sriram et al., 2004; Iyer, Sriram, Westgate, Shanks, unpublished data). This is unlikely to be an artifact of protein hydrolysis or NMR; therefore, it suggests the metabolism of Leu by pathways not considered in our metabolic model (Sriram et al., 2004). Supplementary material 3 shows a hypothesized mechanism of Leu degradation or cycling to account for this anomaly. We wrote and solved bondomer balances for the Leu[γ–δ^1] bondomer in a manner similar to that illustrated for the anaplerotic pathway (see Section 2), and found that the flux of Leu degradation or cycling (v_3 or v_4, Supplementary material 3) was 25.4% of the flux of Leu biosynthesis or incorporation into protein (v_1 or v_2, Supplementary material 3). In plants, Leu is principally catabolized toward the synthesis of fatty acids (Gerbling and Gerhardt, 1989; Anderson et al., 1998; Daschner et al., 1999; van der Hoeven and Steffens, 2000; Fujiki et al., 2001; Schuster and Binder, 2005). A possible degradation route consistent with that hypothesized in Supplemental material 3 is the conversion of Leu to propi-

onyl CoA (Gerbling and Gerhardt, 1989). While this hypothesis needs verification, the anomaly in Leu bondomer abundances emphasizes that comprehensive flux analysis can assist in the elucidation of unknown pathways.

4. Concluding remarks

This article reports the application of bondomers to plant metabolic flux analysis and a comprehensive ^{13}C labeling-based metabolic flux analysis of a plant hairy root system. We showed that bondomers are not only computationally more efficient than isotopomers, but also more intuitively interpretable. Both these features should make bondomer-based flux evaluation broadly applicable in plants, especially in future applications such as instationary flux analysis. The current formulation of the bondomer concept only permits the analysis of labeling experiments that employ a single fractionally U–^{13}C labeled carbon source; isotopomers (or future extensions of the bondomer concept) will have to be used to analyze other kinds of labeling experiments. Currently in our laboratory, we are employing this methodology to assess the impact of genetic or environmental changes in the hairy roots, especially in recently engineered genetic variants of *C. roseus* hairy roots (Hughes et al., 2004a,b; Hong et al., 2006b,a).

5. Experimental

5.1. Hairy root culture

C. roseus LBE-6-1 hairy roots were cultured as described previously (Bhadra and Shanks, 1997) at 26 °C in 50 mL liquid medium containing 30 g L^{-1} sucrose and 1.65 g L^{-1} Gamborg B5 salts (Sigma–Aldrich). The sucrose was either fractionally (5% w/w or 10% w/w) U–^{13}C labeled (Sigma–Aldrich, St. Louis, MO), or unlabeled (0% U–^{13}C; therefore containing only naturally abundant ^{13}C). The growth rate and extracellular fluxes of the 5% U–^{13}C sucrose-grown hairy roots were not significantly different from those of the unlabeled sucrose-grown controls ($p > 0.30$, $n = 4$, see Section 2). However, the hairy root tips transferred to 10% U–^{13}C sucrose media exhibited no lateral branching or growth, callused slightly, and were visually distinguishable from the 5% U–^{13}C sucrose-grown and the unlabeled sucrose-grown controls ($n = 4$). This observation could not be investigated further due to the high cost of U–^{13}C sucrose. Therefore, all subsequent labeling experiments were performed by growing hairy roots in media containing 5% U–^{13}C sucrose.

Hairy roots were harvested at mid-exponential phase (16.5 d) of growth, at which time the dry weight was 0.0775 g $flask^{-1}$. The harvested hairy roots were lyophilized at −50 °C and 133×10^{-6} bar for 72 h, weighed, ground, and stored at −80 °C.

5.2. Aqueous extraction of hairy roots, hydrolysis, and NMR sample preparation

Aqueous extracts (containing protein and β-glucans) of lyophilized, ground hairy roots were prepared by contacting the hairy roots in 100 mM phosphate buffer (pH 7.2) at 4 °C for 15 min, in four stages (with a centrifugation and resuspension between each stage). Protein was detected in the extract by using the Bradford test (Bio-Rad Laboratories, Hercules, CA). The extract was acid hydrolyzed for 4 h at 150 °C in hydrolysis tubes (Pierce Endogen, Rockford, IL) containing 6 N HCl. Before hydrolysis, the tube was evacuated, flushed with nitrogen to remove residual oxygen, and re-evacuated. The acid in the protein hydrolysate was evaporated in a Rapidvap evaporator (Labconco, Kansas City, MO). The residue was re-dissolved in 2 mL deionized water, lyophilized for 72 h, and dissolved in 500 μL D_2O in an NMR tube. The pH of the NMR sample was adjusted to 0.5 using DCl.

5.3. NMR spectroscopy and calculation of bondomer abundances

All NMR spectra were acquired at 298 K on a Bruker Avance DRX 500 MHz spectrometer (Bruker BioSpin, Billerica, MA). The methyl signal of dimethylsilapentanesulfonate (Sigma–Aldrich) was used as an internal standard, and its ^{1}H chemical shift was set to zero ppm.

To measure isotopomer abundances, 2-D [^{13}C, ^{1}H] HSQC spectra were acquired by employing a modified version of the INEPT (insensitive nuclei enhanced by polarization transfer) pulse sequence from Bodenhausen and Ruben (1980). Acquisition parameters were as follows: ^{13}C (F1) resonance frequency, 125.7 MHz; ^{1}H (F2) resonance frequency, 499.9 MHz; spectral width along F1 dimension, 5028.05 Hz (minimized by using peak aliasing); spectral width along F2 dimension, 5482.26 Hz; number of complex data points, 900 (^{13}C) × 1024 (^{1}H); number of scans, 16. Assignment of amino acid peaks on the spectrum was verified using 2-D [^{1}H, ^{1}H] and 3-D [^{13}C, ^{1}H, ^{1}H] TOCSY spectra (Braunschweiler and Ernst, 1983) of a 100% labeled protein sample. To measure ^{13}C atom enrichments, a 2-D [^{1}H, ^{1}H] TOCSY spectrum was acquired by using the DIPSI-2 (decoupling in the presence of scalar interactions-2) sequence (Shaka et al., 1988) for isotropic mixing, with a mixing time of 76 ms.

The software Xwinnmr™ (Bruker BioSpin) was used to acquire all spectra, and the software NMRView™ (Johnson and Blevins, 1994; available at www.onemoonscientific.com) was used to quantify multiplets on the TOCSY spectrum and non-overlapping multiplets on the HSQC spectra. To quantify overlapping multiplets (α-amino acid and LVA peaks) on the HSQC spectra, a peak deconvolution software was written based on a spectral model originally proposed by van Winden et al. (2001). Additionally, 2-D spectra were acquired that were *J*-scaled along the F1 dimension, by incorporating pulse sequences described

by Willker et al. (1997) and Brown (1984) into the HSQC pulse sequence. *J*-scaling increases multiplet separation by an even integral factor *J* and eliminates multiplet overlap. *J*-scaling factors of 6 or 8 were employed. Isotopomer abundances were converted to bondomer abundances by using formulae from Szyperski (1995) and their extensions.

5.4. Extracellular fluxes

Extracellular fluxes (those between the hairy roots and the surrounding liquid medium) were measured by quantifying the metabolites sucrose, glucose, fructose, Pyr, Mal, and succinate in the growth medium. 15 μL of each sample or standard was injected in duplicate into an HPLC system (Waters, Milford, MA) that utilized a carbohydrate analysis column (30 × 3.9 cm, pore size 125 Å) and a refractive index (RI) detector. The mobile phase was a 75:25 mixture of acetonitrile and deionized water. The temperature was maintained at 24 °C and the flow rate was maintained constant at 0.5 mL min^{-1}. Data acquisition and analysis were performed with the Empower™ software (Waters).

5.5. Metabolic flux evaluation

To evaluate fluxes from the measured bondomer abundances and extracellular/biomass synthesis fluxes, we employed our previously reported computer program NMR2Flux (Sriram et al., 2004), which we adapted in this work to utilize bondomer abundance data. Our previous publications provide mathematical details on bondomer balancing (Sriram and Shanks, 2004) and on the working of NMR2Flux (Sriram et al., 2004). Briefly, the version used in this work evaluates fluxes from ^{13}C labeling data by employing comprehensive bondomer balancing and a global optimization (simulated annealing) routine. Further, identifiability of fluxes from the supplied data as well as solution uniqueness were verified, and statistical analysis was performed to calculate standard deviations of the fluxes (Sriram et al., 2004). NMR2Flux accepts metabolic network information (reaction stoichiometries and carbon skeleton rearrangements), bondomer abundances, and extracellular flux/biomass composition data in a spreadsheet format and is therefore generic. It is implemented in the programming language C, on the Red Hat Linux operating system.

5.6. Estimation of errors in measurements and evaluated fluxes, and statistical analysis

The extracellular fluxes and biomass growth rate were measured for four biological replicates, and errors were calculated as the standard deviations of these measurements. Errors in fluxes contributing to biomass synthesis were taken from our previous work (Sriram et al., 2006). To measure isotopomer abundances by 2-D NMR, we pooled the four ^{13}C-grown biological replicates of *C. roseus* hairy roots into a single NMR sample (due to NMR sensitivity and high cost of ^{13}C sucrose). Therefore, the isotopomer abundances reflect the average of those of the four biological replicates, while the errors only include instrumental errors arising due to the NMR spectrometer, and errors arising due to isotopomer quantification procedure. Since isotopomers and bondomers are linearly related, these errors in isotopomer abundances were appropriately converted to errors in bondomer abundances. Errors in evaluated fluxes were estimated from errors in the extracellular fluxes, biomass growth rate, biomass synthesis fluxes, and isotopomer/bondomer abundances by performing a bootstrap Monte Carlo statistical analysis as explained in Press et al. (1992) and in our previous paper (Sriram et al., 2004, Supplementary material IV). Significant differences between results were evaluated by using a Student's *t*-test.

Acknowledgments

This work was funded by National Science Foundation Grant No. BES–0224600. The authors thank Omar González-Rivera (Department of Chemical and Biological Engineering, Iowa State University) for HPLC measurements.

Appendix A. Supplementary data

Supplementary data associated with this article can be found, in the online version, at doi:10.1016/j.phytochem.2007.04.009.

References

Anderson, M.D., Che, P., Song, J., Nikolau, B.J., Wurtele, E.S., 1998. 3-Methylcrotonyl-coenzyme A carboxylase is a component of the mitochondrial leucine catabolic pathway in plants. Plant Physiol. 118, 1127–1138.

Bhadra, R., Shanks, J.V., 1997. Transient studies of nutrient uptake, growth and indole alkaloid accumulation in heterotrophic cultures of *Catharanthus roseus* hairy roots. Biotech. Bioeng. 55, 527–534.

Bodenhausen, G., Ruben, D.J., 1980. Natural abundance nitrogen-15 NMR by enhanced heteronuclear spectroscopy. Chem. Phys. Lett. 69, 185–189.

Braunschweiler, L., Ernst, R.R., 1983. Correlation transfer by isotropic mixing: application to proton correlation spectroscopy. J. Magn. Reson. 53, 521–528.

Brown, L.R., 1984. Differential scaling along ω_1 in COSY experiments. J. Magn. Reson. 57, 513–518.

Chollet, R., Vidal, J., O'Leary, M.H., 1996. Phospho*enol* pyruvate carboxylase: a ubiquitous, highly regulated enzyme in plants. Annu. Rev. Plant Physiol. Plant Mol. Biol. 47, 273–298.

Daschner, K., Thalheim, C., Guha, C., Brennicke, A., Binder, S., 1999. In plants a putative isovaleryl-CoA-dehydrogenase is located in mitochondria. Plant Mol. Biol. 39, 1275–1282.

Entwistle, G., ap Rees, T.A., 1990. Lack of fructose-1:6-bisphosphatase in a range of higher plants that store starch. Biochem. J. 271, 467–472.

Fell, D.A., 2005. Enzymes, metabolites and fluxes. J. Exp. Bot. 56, 267–272.

Fernie, A.R., Geigenberger, P., Stitt, M., 2005. Flux an important, but neglected, component of functional genomics. Curr. Opin. Plant. Biol. 8, 174–182.

Fiaux, J., Andersson, C.I.J., Holmberg, N., Bulow, L., Kallio, P.T., Szyperski, T., Bailey, J.E., Wuthrich, K., 1999. C-13 NMR flux ratio analysis of *Escherichia coli* central carbon metabolism in microaerobic bioprocesses. J. Am. Chem. Soc. 121, 1407–1408.

Fujiki, Y., Ito, M., Nishida, I., Watanabe, A., 2001. Leucine and its keto acid enhance the coordinated expression of genes for branched-chain amino acid catabolism in *Arabidopsis* under sugar starvation. FEBS Lett. 499, 161–165.

Gerbling, H., Gerhardt, B., 1989. Peroxisomal degradation of branched-chain 2-oxo acids. Plant Physiol. 91, 1387–1392.

Guillet, G., Poupart, J., Basurco, J., De Luca, V., 2000. Expression of tryptophan decarboxylase and tyrosine decarboxylase genes in tobacco results in altered biochemical and physiological phenotypes. Plant Physiol. 122, 933–944.

Harris, R.K., 1983. Nuclear Magnetic Resonance Spectroscopy. A Physicochemical View. Pitman Books, London.

Hong, S.B., Peebles, C.A., Shanks, J.V., San, K.Y., Gibson, S.I., 2006a. Expression of the *Arabidopsis* feedback-insensitive anthranilate synthase holoenzyme and tryptophan decarboxylase genes in *Catharanthus roseus* hairy roots. J. Biotechnol. 122, 28–38.

Hong, S.B., Peebles, C.A., Shanks, J.V., San, K.Y., Gibson, S.I., 2006b. Terpenoid indole alkaloid production by *Catharanthus roseus* hairy roots induced by *Agrobacterium tumefaciens* harboring *rolABC* genes. Biotech. Bioeng. 93, 386–390.

Hughes, E.H., Hong, S.-B., San, K.-Y., Gibson, S.I., Shanks, J.V., 2004a. Expression of a feedback-resistant anthranilate synthase in *Catharanthus roseus* hairy roots provides evidence for tight regulation of terpenoid indole alkaloid levels. Biotech. Bioeng. 86, 718–727.

Hughes, E.H., Hong, S.-B., San, K.-Y., Gibson, S.I., Shanks, J.V., 2004b. Metabolic engineering of the indole pathway in *Catharanthus roseus* hairy roots leads to increases in tryptamine and serpentine accumulation. Metab. Eng. 6, 268–276.

Hughes, E.H., Hong, S.B., Gibson, S.I., Shanks, J.V., San, K.Y., 2004c. Expression of a feedback-resistant anthranilate synthase in *Catharanthus roseus* hairy roots provides evidence for tight regulation of terpenoid indole alkaloid levels. Biotech. Bioeng. 86, 718–727.

Iyer, V.V., Sriram, G., Shanks, J.V., 2007. Metabolic flux quantification of central carbon metabolism in plant systems. In: Nikolau, B.J., Wurtele, E.S. (Eds.), Concepts in Plant Metabolomics. Springer.

Johnson, B.A., Blevins, R.A., 1994. NMRView: a computer program for the visualization and analysis of NMR data. J. Biomol. NMR 4, 603–614.

King, L.M., Opie, L.H., 1998. Glucose and glycogen utilisation in myocardial ischemia-changes in metabolism and consequences for the myocyte. Mol. Cell. Biochem. 180, 3–26.

Klapa, M.I., Park, S.M., Sinskey, A.J., Stephanopoulos, G., 1999. Metabolite and isotopomer balancing in the analysis of metabolic cycles: I. Theory. Biotechnol. Bioeng. 62, 375–391.

Kruger, N.J., Ratcliffe, R.G., Roscher, A., 2003. Quantitative approaches for analysing fluxes through plant metabolic networks using NMR and stable isotope labelling. Phytochem. Rev. 2, 17–30.

Lange, B.M., 2006. Integrative analysis of metabolic networks: from peaks to flux models? Curr. Opin. Plant Biol. 9, 220.

Nöh, K., Wiechert, W., 2006. Experimental design principles for isotopically instationary ^{13}C labeling experiments. Biotech. Bioeng. 94, 234–251.

Press, W.H., Teukolsky, S.A., Wetterling, W.T., Flannery, B.P., 1992. Numerical Recipes in C: The Art of Scientific Computing. Cambridge University Press, Cambridge, UK.

Ratcliffe, R.G., Shachar-Hill, Y., 2001. Probing plant metabolism with NMR. Annu. Rev. Plant Physiol. Plant Mol. Biol. 52, 499–526.

Ratcliffe, R.G., Shachar-Hill, Y., 2005. Revealing metabolic phenotypes in plants: inputs from NMR analysis. Biol. Rev. 80, 27–43.

Ratcliffe, R.G., Shachar-Hill, Y., 2006. Measuring multiple fluxes through plant metabolic networks. Plant J. 45, 490–511.

Rhee, S.Y., Dickerson, J., Xu, D., 2006. Bioinformatics and its applications in plant biology. Annu. Rev. Plant Biol. 57, 335–360.

Rontein, D., Dieuaide-Noubhani, M., Dufourc, E.J., Raymond, P., Rolin, D., 2002. The metabolic architecture of plant cells. Stability of central metabolism and flexibility of anabolic pathways during the growth cycle of tomato cells. J. Biol. Chem. 277, 43948–43960.

Sauer, U., 2004. High-throughput phenomics: experimental methods for mapping fluxomes. Curr. Opin. Biotechnol. 15, 58–63.

Sauer, U., Lasko, D.R., Fiaux, J., Hochuli, M., Glaser, R., Szyperski, T., Wuthrich, K., Bailey, J.E., 1999. Metabolic flux ratio analysis of genetic and environmental modulations of *Escherichia coli* central carbon metabolism. J. Bacteriol. 181, 6679–6688.

Schlatmann, J.E., Koolhaas, C.M.A., Vinke, J.L., ten Hoopen, H.J.G., Heijnen, J.J., 1995. The role of glucose in ajmalicine production by *Catharanthus roseus* cell cultures. Biotech. Bioeng. 47, 525–534.

Schmidt, K., Nørregaard, L.C., Pedersen, B., Meissner, A., Duus, J.O., Nielsen, J.O., Villadsen, J., 1999. Quantification of intracellular metabolic fluxes from fractional enrichment and ^{13}C–^{13}C coupling constraints on the isotopomer distribution in labeled biomass components. Metab. Eng. 1, 166.

Schuster, J., Binder, S., 2005. The mitochondrial branched-chain aminotransferase (AtBCAT-1) is capable to initiate degradation of leucine, isoleucine and valine in almost all tissues in *Arabidopsis* thaliana. Plant Mol. Biol. 57, 241–254.

Schwender, J., Goffman, F., Ohlrogge, J.B., Shachar-Hill, Y., 2004a. Rubisco without the Calvin cycle improves the carbon efficiency of developing green seeds. Nature 432, 779–782.

Schwender, J., Ohlrogge, J., Shachar-Hill, Y., 2004b. Understanding flux in plant metabolic networks. Curr. Opin. Plant Biol. 7, 309–317.

Schwender, J., Ohlrogge, J.B., Shachar-Hill, Y., 2003. A flux model of glycolysis and the oxidative pentosephosphate pathway in developing *Brassica napus* embryos. J. Biol. Chem. 278, 29442–29453.

Schwender, J., Shachar-Hill, Y., Ohlrogge, J.B., 2007. Mitochondrial metabolism in developing embryos of *Brassica napus*. J. Biol. Chem. 281, 34040–34046.

Shaka, A.J., Lee, C.J., Pines, R.A., 1988. Iterative schemes for bilinear operators: applications to spin decoupling. J. Magn. Reson. 77, 274–293.

Shanks, J.V., 2005. Phytochemical engineering: combining chemical reaction engineering with plant science. AIChE J. 51, 2–7.

Singh, B.K., 1999. Plant Amino Acids: Biochemistry and Biotechnology. Marcel-Dekker, New York.

Spielbauer, G., Margl, L., Hannah, L.C., Römisch, W., Ettenhuber, C., Bacher, A., Gierl, A., Eisenreich, W., Genschel, U., 2006. Robustness of central carbohydrate metabolism in developing maize kernels. Phytochemistry 67, 1460–1475.

Sriram, G., Fulton, D.B., Iyer, V.V., Peterson, J.M., Zhou, R., Westgate, M.E., Spalding, M.H., Shanks, J.V., 2004. Quantification of compartmented metabolic fluxes in developing soybean embryos by employing biosynthetically directed fractional ^{13}C labeling, two-dimensional [^{13}C, ^{1}H] nuclear magnetic resonance, and comprehensive isotopomer balancing. Plant Physiol. 136, 3043–3057.

Sriram, G., González-Rivera, O., Shanks, J.V., 2006. Determination of biomass composition of *Catharanthus roseus* hairy roots for metabolic flux analysis. Biotechnol. Prog. 22, 1659–1663.

Sriram, G., Shanks, J.V., 2001. A mathematical model for carbon bond labeling experiments: Analytical solutions and sensitivity analysis for the effect of reaction reversibilities on estimated fluxes. In: Erickson, L.E. (Ed.), 31st Annual Biochemical Engineering Symposium. Manhattan, KS, pp. 45–54.

Sriram, G., Shanks, J.V., 2004. Improvements in metabolic flux analysis using carbon bond labeling experiments: bondomer balancing and Boolean function mapping. Metab. Eng. 6, 116–132.

Stephanopoulos, G., 1999. Metabolic fluxes and metabolic engineering. Metab. Eng. 1, 1–11.

Stephanopoulos, G., 2002. Metabolic engineering: perspective of a chemical engineer. AIChE J. 48, 920–926.

Stephanopoulos, G., Stafford, D.E., 2002. Metabolic engineering: a new frontier of chemical reaction engineering. Chem. Eng. Sci. 57, 2595–2602.

Sweetlove, L.J., Fernie, A.R., 2005. Regulation of metabolic networks: understanding metabolic complexity in the systems biology era. New Phytol. 168, 9–23.

Sweetlove, L.J., Last, R.L., Fernie, A.D., 2003. Predictive metabolic engineering: a goal for systems biology. Plant Physiol. 132, 420–425.

Szyperski, T., 1995. Biosynthetically directed fractional ^{13}C-labeling of proteinogenic amino acids. Eur. J. Biochem. 232, 433–448.

Szyperski, T., 1998. ^{13}C NMR, MS, and metabolic flux balancing in biotechnology research. Q. Rev. Biophys. 31, 41–106.

van der Hoeven, R.S., Steffens, J.C., 2000. Biosynthesis and elongation of short- and medium-chain-length fatty acids. Plant Physiol. 122, 275–282.

van Gulik, W.M., de Laat, W.T., Vinke, J.L., Heijnen, J.J., 2000. Application of metabolic flux analysis for the identification of metabolic bottlenecks in the biosynthesis of penicillin-G. Biotech. Bioeng. 68, 602–618.

van Winden, W., Schipper, D., Verheijen, P., Heijnen, J., 2001. Innovations in generation and analysis of 2D [^{13}C, ^{1}H] COSY NMR spectra for metabolic flux analysis purposes. Metab. Eng. 3, 322–343.

van Winden, W.A., Verheijen, P., Heijnen, J.J., 2002. Cumulative bondomers: a new concept in flux analysis from 2D [^{13}C, ^{1}H] COSY data. Biotech. Bioeng. 80, 731–745.

Wheeler, G.L., Jones, M.A., Smirnoff, N., 1998. The biosynthetic pathway of vitamin C in higher plants. Nature 393, 365–369.

Wiechert, W., Nöh, K., 2005. From stationary to instationary metabolic flux analysis. Adv. Biochem. Eng. Biotechnol. 92, 145–172.

Willker, W., Flögel, U., Leibfritz, D., 1997. Ultra-high resolved HSQC spectra of multiple ^{13}C-labeled biofluids. J. Magn. Reson. 125, 216–219.

Zoglowek, C., Kromer, S., Heldt, H.W., 1988. Oxaloacetate and malate transport by plant mitochondria 1. Plant Physiol. 87, 109–115.